Supporting Information

Popa et al. 10.1073/pnas.0913016107

SI Materials and Methods

Behavioral states of vigilance were scored using Somnologica (Flaga) in accordance with previously established criteria in rats (1). Unit and local field potential (LFP) activity was initially sampled at 25 kHz and stored on a hard drive for offline analysis.

Eight wires were inserted in each structure to ensure mechanical rigidity of the bundle (and therefore straight trajectory upon insertion in the brain). However, only two to four of the eight wires were connected to the headstage. The LFPs were very similar across wires belonging to the same bundle. For coherence analysis, we therefore used the average coherence spectra from the connected wires. For Granger analysis, which is more computationally intensive, we picked one channel randomly.

Power spectral density estimates were obtained with the Welch method with 2-s windows overlapping 1 s from the signal downsampled to 500 Hz. Coherence estimates were obtained from cross-power spectra density estimates of pairs of LFP recordings, using the same parameters. Changes in coherence are computed as the difference in the summed coherence in the frequency band of interest. There was no relationship between the duration of posttraining paradoxical sleep (PS) episodes and the changes in theta LFP coherence for both basolateral amygdala–hippocampus (BLA-Hi) ($r = 0.23$, $P = 0.55$) or BLA–medial prefrontal cortex (BLA-mPFC) ($r = 0.34$, $P = 0.36$), and a correlation between the latency of post-PS epochs (36.1 ± 2.4 min) and the changes in coherence of BLA-Hi theta ($r = 0.74$, $P = 0.024$) but not BLA-mPFC theta ($r = 0.26$, $P = 0.5$).

To compute the correlation between the amplitude of theta oscillations in the BLA-Hi-mPFC network, the LFP was band-pass filtered (6–8 Hz), the peaks of theta oscillations were detected in each structure, and a regression was performed by pairing the peak amplitudes in one structure to the amplitudes of the nearest peaks in the other structures.

Unit entrainment by theta was assessed during periods of high-amplitude theta identified by a continuous wavelet transform with Morlet wavelets, with ≥25% of the 0–10-Hz band power contained in the 6–8-Hz range. For each cell, the uniformity of the phase distribution was then tested with a Rayleigh test. The probability values for all of the cells were then adjusted for multiple comparisons. The phase distribution for the cells exhibiting significant theta entrainment was fitted with a von Mises distribution to determine the preferred phase.

Wavelet periodograms and coherence were computed with Morlet wavelets, using the package Sowas (http://tocsy.agnld.uni-potsdam.de/wavelets/) (2). Local estimates of wavelet coherence in the time-frequency plane were computed over a time-frequency domain of ± 1/4 octave in the frequency direction and ±2 periods in the time direction around each point.

Granger causality analysis (3, 4) was used to study the directionality of interactions between brain areas. Granger spectra were computed using the BSMART Matlab package (5).The PS LFP traces during periods of high amplitude theta, isolated as for phase-locking analysis (see above), were downsampled to 125 Hz and split into 1-s epochs with substraction of the temporal mean and normalization of the variance. Adaptive multivariate auto regressive (AMAR) modeling was obtained from the Levinson-Wiggins-Robinson algorithm (5). The order of the model was established using the minimal values of the Akaike information criterion, indicating an optimal number of parameters. Minima were found in the interval 11–15, but for some recording sessions in which no minimal value was found for the range of orders considered (1–18), we used models of order 15 because a reduction of the slope for orders beyond this value was observed (Fig. S5*A*), indicating a reduced benefit of adding parameters beyond this value. The number of parameters in the AMAR models corresponds to the number of time lags included, which in our case correspond to up to 120 ms, approximately the duration of one theta cycle. All models were stable (negative stability index), and the consistency test (5) indicated that a large fraction [mean ± SD (min–max): 95.5% ± 2.2% (88.6–97.9%)] of the variance of the data were captured by the models. The resemblance of the spectral estimates from the AMAR model with Welch's estimates of the power spectra and coherence of the normalized data was verified (Fig. S5 *B* and *C*). Significance of peaks in Granger spectra was obtained by generating 1,000 shuffled datasets in which 1-s epochs of each recording sites were independently permuted. Granger analysis was performed for each of these shuffled datasets. The original peak in the theta band of each Granger spectra was then compared with the distribution of the peak amplitude in the theta band obtained from the shuffling procedure, to test whether it occurred by chance. Peaks with amplitude larger than the highest fifth percentile ($P = 0.05$) were considered significant, and only peaks with significant amplitude were considered to indicate a directional influence in the theta frequency band.

1. Gervasoni D, et al. (2004) Global forebrain dynamics predict rat behavioral states and their transitions. *J Neurosci* 24:11137–11147.
2. Maraun D, Kurths J (2004) Cross wavelet analysis. Significance testing and pitfalls. *Nonlinear Processes Geophys* 11:505–514.
3. Geweke J (1982) Measurements of linear-dependance and feedback between multiple time-series. *J Am Stat Assoc* 77:304–313.
4. Granger CWJ (1969) Investigating causal relations by economic models and cross-spectral methods. *Econometrica* 37:424–438.
5. Cui J, Xu L, Bressler SL, Ding M, Liang H (2008) BSMART: A Matlab/C toolbox for analysis of multichannel neural time series. *Neural Netw* 21:1094–1104.

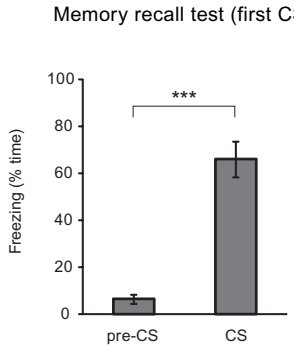

Fig. S1. Comparison between freezing levels before vs. during the first conditioned stimulus (CS) of the recall test. Graph showing percentage time spent freezing (*y* axis) during the 20 s preceding the first CS (left bar) and during the first CS (right bar). The average percentage time freezing ± SEM for the 20 s before the first CS presentation of the memory recall test (6.67 ± 1.88) was not significantly different from before conditioning ($P = 0.65$) but was different from the freezing during the first CS presentation of the recall test (66.25 ± 7.71; $P < 0.0001$). This indicates that conditioning occurred and that conditioning was to the tone.

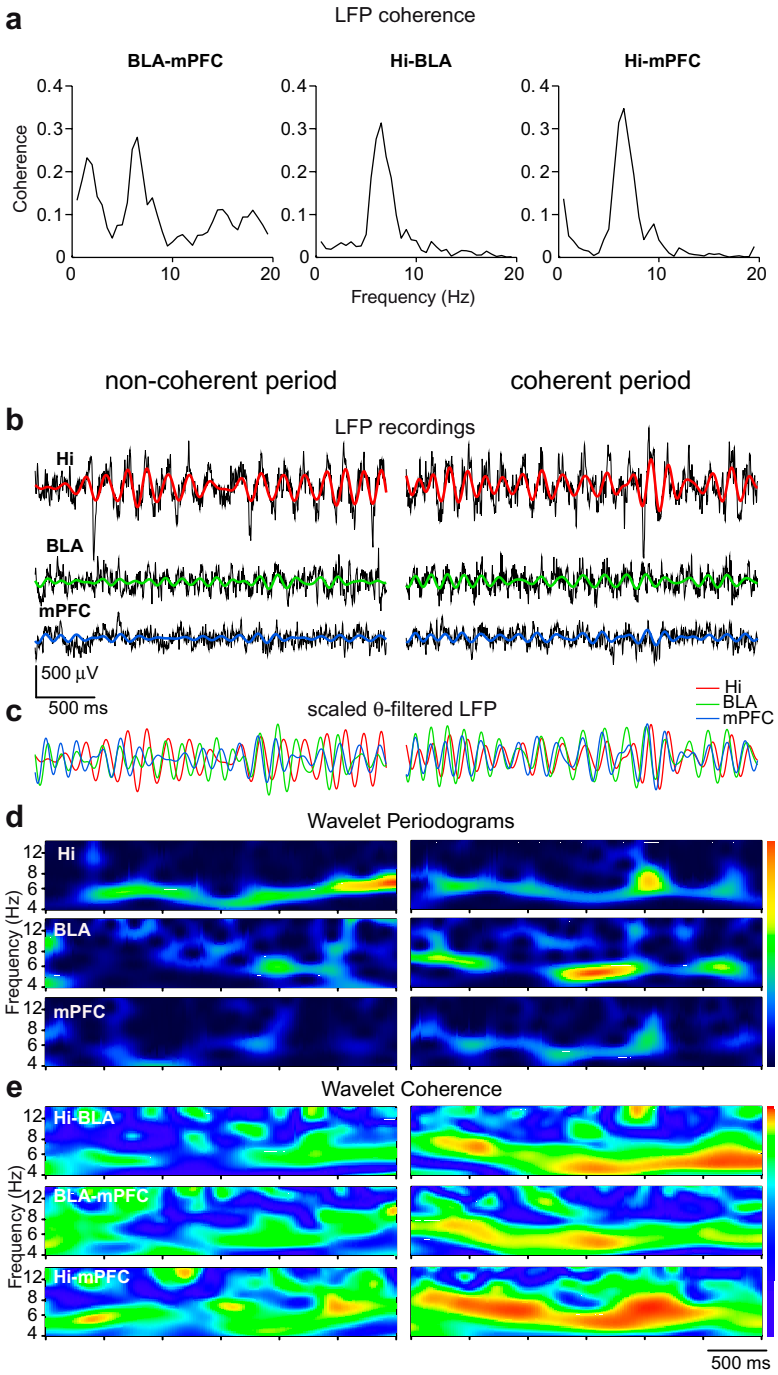

Fig. S2. Intermittent coherence in the theta band in the Hi-BLA-mPFC network. (*A*) Examples of coherence spectra. (*B–E*) Example of noncoherent (*Left*) and a coherent (*Right*) PS period from one animal: (*B*) LFP recordings, (*C*) scaled theta filtered LFP (5–8 Hz), (*D*) wavelet periodograms for Hi, BLA, and mPFC, and (*E*) wavelet coherence spectra between Hi-BLA, BLA-mPFC, and Hi-mPFC. Consistent phase relations between the traces are clearly observed in the scaled filtered LFP traces and in the coherence spectra of the "coherent" but not the "noncoherent" period (whereas both exhibit strong hippocampal theta oscillations). (Scale bar for wavelet periodograms corresponds to the range 0–80 μV for BLA and mPFC and to the range 0–660 μV for Hi. Wavelet coherence scale bar corresponds to 0–1.)

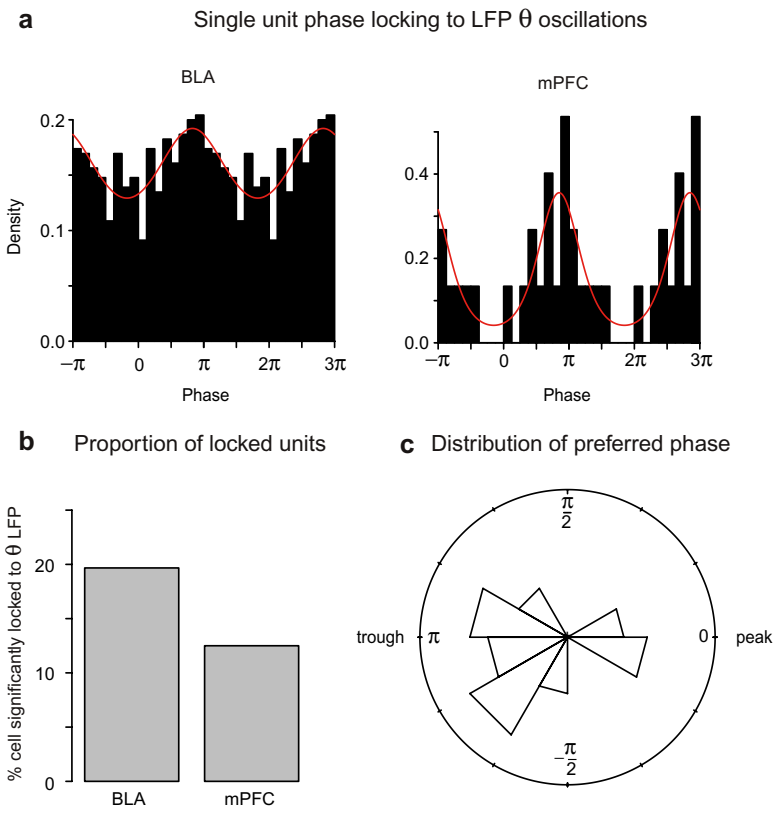

Fig. S3. (*A*) Phase distribution of spikes during local theta oscillations for a BLA (*Left*) and mPFC (*Right*) single unit. Red line: von Mises distribution fit to the phase distribution. 0 corresponds to the positive peak of theta oscillation. (*B*) Percentage of cells with significant phase-locked firing to theta in each structure. (*C*) Distribution of preferred phase for all cells with significant theta phase-locking. Note that the preferred phase predominantly occurred in the trough of the oscillations (around π).

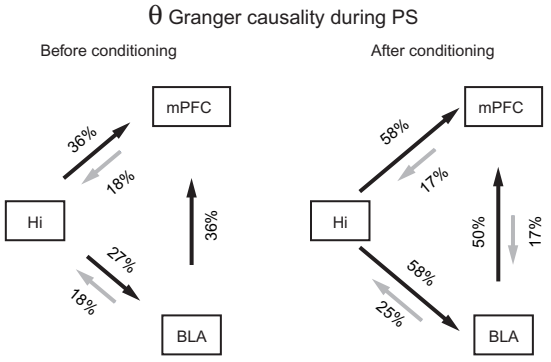

Fig. S4. Summary of the causal influences inferred from the Granger analyses in the Hi-mPFC-BLA network during PS before (*Left*) and after (*Right*) conditioning. Data are expressed as proportion of animals exhibiting a predominant causal influence of one structure on another in the Hi-mPFC-BLA network (e.g., theta-band peak amplitude in Hi → BLA spectrum larger than in BLA → Hi spectrum). Animals with no peaks in the theta band are not represented. Dark arrows correspond to the most frequently observed pattern.

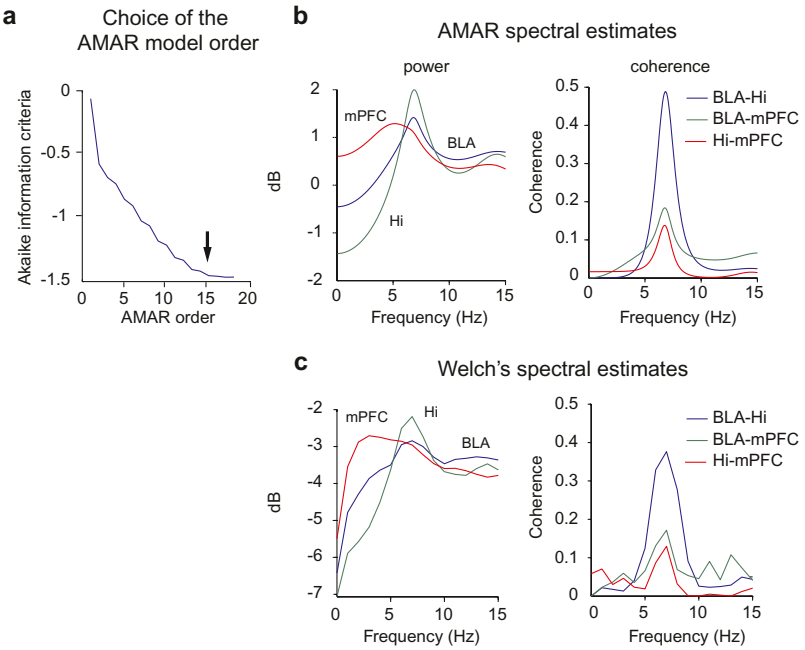

Fig. S5. AMAR modeling of the normalized data for Granger analysis (same example as in Fig. S4*A*). (*A*) Example of Akaike information criteria as a function of model order. A reduced slope is found for orders beyond 15 (arrow), indicating a reduced benefit in adding parameters to the AMAR model beyond this value. (*B*) Examples of estimates from the AMAR model of the spectral content (*Left*) and of spectral coherence between structures (*Right*). (*C*) Welch's spectral estimates of spectral content (*Left*) and coherence (*Right*) between structures from the same example as *B*.

Table S1. Pearson correlation coefficients (*r*) and significance (*P*) values for linear regressions between change in wakefulness, slow-wave sleep (SWS), and PS coherence in different frequency bands between BLA and Hi or BLA and mPFC and overnight consolidation

	BLA-Hi			BLA-mPFC		
Frequency band	Wake	SWS	PS	Wake	SWS	PS
delta	$r = 0.39$	$r = 0.51$	$r = 0.32$	$r = 0.25$	$r = 0.38$	$r = 0.10$
	$P = 0.234$	$P = 0.094$	$P = 0.344$	$P = 0.461$	$P = 0.228$	$P = 0.774$
theta	$r = 0.33$	$r = 0.29$	$r = 0.67$	$r = 0.25$	$r = 0.42$	$r = 0.81$
	$P = 0.330$	$P = 0.357$	$P = 0.025$*	$P = 0.463$	$P = 0.174$	$P = 0.003$*
beta	$r = 0.32$	$r = 0.18$	$r = 0.23$	$r = 0.19$	$r = 0.12$	$r = 0.32$
	$P = 0.336$	$P = 0.583$	$P = 0.489$	$P = 0.579$	$P = 0.702$	$P = 0.346$
low gamma	$r = 0.11$	$r = 0.04$	$r = 0.07$	$r = 0.02$	$r = 0.24$	$r = 0.10$
	$P = 0.738$	$P = 0.900$	$P = 0.837$	$P = 0.948$	$P = 0.444$	$P = 0.779$
high gamma	$r = 0.14$	$r = 0.34$	$r = 0.27$	$r = 0.15$	$r = 0.22$	$r = 0.17$
	$P = 0.680$	$P = 0.278$	$P = 0.419$	$P = 0.671$	$P = 0.492$	$P = 0.611$

Delta: 0–3 Hz; theta: 6–8 Hz; beta: 10–30 Hz; low gamma: 30–50 Hz; and high gamma: 65–100 Hz.
*Significant relationship at 0.003 level.

Table S2. ANOVA for prediction of consolidation success

Variable	df	Sum Sq	Mean Sq	*F*	*Pr*(>*F*)	
BLA-Hi						
Δcoherence	1	2178.46	2178.46	7.1206	0.03207	*
Freezing last FC trial	1	0.7	0.7	0.0023	0.96312	
Freezing TH (5 trials)	1	570.28	570.28	1.864	0.21441	
Residuals	7	2141.56	305.94			
BLA-mPFC						
Δcoherence	1	3038.61	3038.61	12.8277	0.008957	†
Freezing last FC trial	1	13.63	13.63	0.0575	0.817297	
Freezing TH (5 trials)	1	180.6	180.6	0.7624	0.41152	
Residuals	7	1658.15	236.88			
BLA-Hi						
Δcoherence	1	2178.46	2178.46	7.3518	0.03014	*
PS latency	1	276.71	276.71	0.9338	0.36606	
PS duration	1	361.6	361.6	1.2203	0.30582	
Residuals	7	2074.22	296.32			
BLA-mPFC						
Δcoherence	1	3038.61	3038.61	12.6006	0.009347	†
PS latency	1	22	22	0.0912	0.771419	
PS duration	1	142.36	142.36	0.5903	0.467416	
Residuals	7	1688.03	241.15			

Note that the interindividual variations of consolidation are explained by changes in theta coherence between the BLA and Hi or the BLA and mPFC, even when taking into account the interindividual variability in behavior [tone habituation (TH) and last fear conditioning (FC) trial] or in PS parameters (duration and latency).
*Indicates significant effect at 0.05 level.
†Indicates significant effect at 0.01 level.

Table S3. ANOVA on Granger preferred direction

Directionality	df	Sum Sq	Mean Sq	*F*	*P*	
Hi → BLA						
After FC	1	2520.61	2520.61	9.3033	0.01582	*
Before FC	1	202.9	202.9	0.7489	0.41203	
Residuals	8	2167.49	270.94			
BLA → mPFC						
After FC	1	2018.48	2018.48	5.7782	0.04292	*
Before FC	1	77.9	77.9	0.223	0.64939	
Residuals	8	2794.62	349.33			
Hi → mPFC						
After FC	1	59.3	59.3	0.1014	0.7584	
Before FC	1	148.7	148.7	0.254	0.6279	
Residuals	8	4683	585.4			

Directions of Granger interactions after, but not before, fear conditioning (FC) are predicting the consolidation for BLA → mPFC and HI → BLA predominant causality influence.
*Indicates significant effect at 0.05 level.